Detection and Tracking of Traffic Signs Using a Recursive Bayesian Decision Framework

Javier Marinas, Luis Salgado, Jon Arróspide, and Marcos Nieto

Abstract— **In this paper we propose a new method for the automatic detection and tracking of road traffic signs using an on-board single camera. This method aims to increase the reliability of the detections such that it can boost the performance of any traffic sign recognition scheme. The proposed approach exploits a combination of different features, such as color, appearance, and tracking information. This information is introduced into a recursive Bayesian decision framework, in which prior probabilities are dynamically adapted to tracking results. This decision scheme obtains a number of candidate regions in the image, according to their HS (Hue-Saturation). Finally, a Kalman filter with an adaptive noise tuning provides the required time and spatial coherence to the estimates. Results have shown that the proposed method achieves high detection rates in challenging scenarios, including illumination changes, rapid motion and significant perspective distortion.**

I. Introduction

AUTOMATIC characterization and recognition of road traffic signs appears as a very attractive topic of research in the field of advanced driver assistance systems. The complexity of the environment, which is continuously changing, as well as the real-time operation requirement, constitute major challenges in this field. Although many different approaches have been proposed in the literature to address traffic sign recognition [1], [6], [9], [11], their performance highly depends on the ability to previously detect and characterize them in the images. Traffic sign detection needs to be done swiftly as soon as signs are visible, while also being robust to illumination changes and perspective distortion, so that time consuming recognition engines [1], [6] can operate after detection.

Detection methods in the literature can be divided into three main groups: color-based, shape-based and those which combine both color and shape information. Color analysis has been exploited in many different ways. For instance, in [1] the authors propose a technique based on static thresholds in RGB space. A similar framework is proposed in [2], [12], where thresholds are applied in HSV space. Although they are very fast, these techniques are not able to cope with significant color variations due to changes in illumination. To improve the performance, more complex color models have been proposed. In [7] a Mixture of Gaussians (MoG)-based color detection is used, in which several Gaussians are employed in order to model different illumination conditions in CIELab color space. Similarly, in [6] a Bayesian approach is used to detect road signs, where likelihood is modeled as a one-dimensional Gaussian distribution applied on the H component of HSI space irrespective of the illumination conditions.

On the other hand, proposed shape-based detection systems typically work with grayscale rather than color images. The most common techniques are based on the extraction of edge or corner points. For instance, Hough Transform is used in [4] and Canny detector is utilized in [11]. In [8] the authors propose a method based on the Fast Radial Symmetry Transform, in order to look for signs of several shapes (circular, triangular, octagonal, etc.). All these techniques show severe limitations when traffic signs appear on cluttered backgrounds, which are particularly frequent in urban environments.

Finally, other authors consider the combination of color and shape information as the best way to strengthen their algorithms. Particularly, in [10], after a color-based segmentation in HSI space, a connected component labeling process is carried out in order to find objects in the image. Once the objects are found, a fuzzy shape descriptor is applied to determine whether the road sign is circular or triangular. In [9] the authors apply two Look-up-tables (LUT) for both H and S components of HSI space. Then, the authors classify the shape of the object comparing the FFT of the signature of the object with that of several reference shapes.

In contrast to intra-frame detection, other authors propose to use previous information to accomplish sign detection. Thereby, instantaneous detection failures (due to occlusion, for example) can be overcome. This involves the design of a temporal tracking stage, which is usually addressed by means of Kalman filters [5] or particle filters [7].

In this paper an innovative approach to traffic sign detection is presented based on the fusion of multiple features operating at both pixel and region level, and the incorporation of an efficient Kalman-based tracking scheme. Detection at pixel level is based on H-S color analysis through an innovative MoG model in a Bayesian decision framework, which also considers different illumination conditions and the presence of misleading elements (brick-like and sky). At region level, a simplified appearance model is used to decrease false positive rates, and a Kalman-based tracking strategy is proposed to ensure detection by taking into account features temporal coherence and the traffic signs appearance evolution. Previous detection results are used to adapt prior information in the color classification stage, and a novel

Manuscript received April 8, 2011. This work has been partially supported by the Ministerio de Ciencia e Innovación of the Spanish Government under projects TEC2007-67764 (SmartVision) and TEC2010-20412 (Enhanced 3DTV).

Javier Marinas, Luis Salgado and Jon Arróspide are with the Grupo de Tratamiento de Imágenes of the Universidad Politécnica de Madrid, 28040, Spain (phone: +34 913367353; fax: +34 913367353; e-mail: {jmm, lsa, jal}@gti.ssr.upm.es).

Marcos Nieto is with Vicomtech-IK4, Research Alliance, San Sebastián, 20009, Spain (phone: +34 943309230; fax: +34 943309393; e-mail: mnieto@vicomtech.org).

approach to model noise in the Kalman filter framework is considered that improves detection accuracy by considering the sign-to-vehicle distance evolution. Excellent results are shown under different illumination conditions, both in highways and urban environments, for blue and red traffic sign detection.

II. System Overview

The block diagram of the system is depicted in Fig. 1. Traffic sign detection is divided into two phases: hypothesis generation and hypothesis verification. In the former, color and appearance information of traffic signs (TS) is analyzed in order to provide a set of regions of interest (ROI) which may contain road signs. After the pre-processing stage (that involves noise reduction, image resizing and RGB to HSV conversion), a Bayesian classifier is used based on a color modeling space in which three illumination conditions are considered: excellent, regular and poor. As a result, pixels in the image are assigned to the class they are more likely to belong to. This pixel-wise classification is used to undertake a connected components analysis in which characterization at region level is carried out. Based on this characterization, a set of candidates is generated holding those compact regions that match the expected TS appearance model (defined in terms of TS area, pictogram area and aspect ratio). In the verification stage, each one of these regions is tracked independently by means of a Kalman filter which, based on an adaptive tuning of the process and measurement noise, provides information to the decision module. In this module the TS area evolution (sign and pictogram) and the trajectory smoothness constraints are taken into account to select the final set of regions to be delivered for classification. Naturally, regions that do not match the expected dynamic patterns (TS size and trajectory evolution) are discarded, while the rest of ROIs are refined, both in location and dimensions, for further classification.

III. Color Analysis

In this stage we separate road signs from the background through color analysis taking into account the H and S components of HSV space [1]. In particular, most TSs feature red or blue borders. Thus, the posterior probability ($P(X_i|\boldsymbol{z})$) of a pixel $\boldsymbol{z} = \{z_H, z_S\}$ to belong to the class $X_i \in \{Red\ (R), Blue\ (B), Background(BG)\}$ is computed using the Bayes' rule as:

$$P(X_i|\boldsymbol{z}) = \frac{p(\boldsymbol{z}|X_i)\,P(X_i)}{p(\boldsymbol{z})} \tag{1}$$

where $p(\boldsymbol{z}|X_i)$ is the likelihood of a pixel $\mathbf{z}$ to belong to a class X_i, $P(X_i)$ is the *a priori* probability of class X_i, and $p(\boldsymbol{z})$ is the evidence. Initially $P(X_i)$ are assumed to be constant and equal for each class. However, as will be explained in Section V, *a priori* probabilities will change dynamically according to the information fed back from the tracking stage. As in [1], we assume that H and S involve independent distributions for all the three classes:

$$p(\boldsymbol{z}|X_i) = p(z_H|X_i)\,p(z_S|X_i) \tag{2}$$

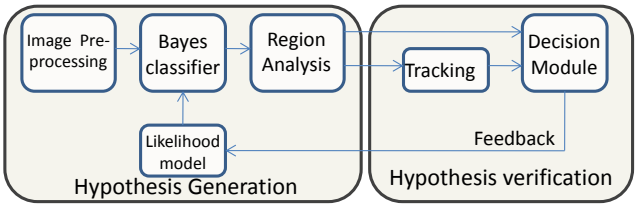

Fig. 1. Block diagram of the proposed TS detection and tracking system.

The likelihood functions $p(z_k|X_i)$, $k \in \{H, S\}$ and $i \in \{R, B\}$, are modeled as a mixture of three Gaussians, each one modeling a different illumination condition: excellent (x), regular (r) and poor (p):

$$p(z_k|X_i) = \frac{1}{3}\sum_{j\in\{x,r,p\}} \frac{1}{\sigma_j\sqrt{2\pi}}\, e^{-\frac{1}{2}\left(\frac{z-\mu_j}{\sigma_j}\right)^2} \tag{3}$$

where μ_j and σ_j vary depending on k and i (explicit references to them have been removed for clarity). The initial parameters (μ, σ) of the mixtures in (3) are obtained through an offline training stage where real road sign images under different illuminations have been considered. The resulting MoGs are presented in Fig. 2. As can be observed, with regards to saturation feature, likelihoods for red (b) and blue (d) TSs show a similar behavior, whereas hue components, (a) and (c), are very discriminative as they cover completely different ranges. Specifically, while for blue TSs the range of H values (c) is concentrated around 0.55, for red TSs (a), valid pixel values are either concentrated in the lower or upper part of the valid range (0,1), thus forcing to model both ranges independently.

In order to model the likelihood function for the background class, $p(z_k|X_{BG})$, a uniform distribution can naturally be assumed. However, there are some elements that are especially frequent in the background of this kind of environments. Particularly relevant are the bricks (or brick-like elements) and the sky, which have a similar color to the objects of interest, i.e. the traffic signs, and can therefore lead to errors unless a special treatment is given to them. In particular, we propose to model the background as a mixture between a uniform distribution and specific functions for the bricks and the sky.

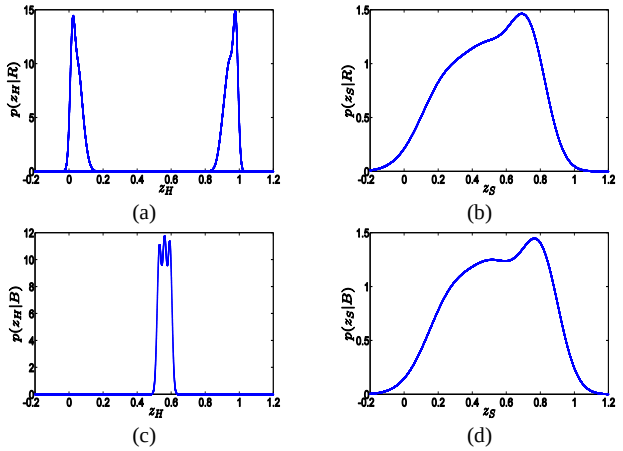

Fig. 2. Designed MoG for each class, for features z_H and z_S: (a) red class, feature z_H, (b) red class, feature z_S, (c) blue class, feature z_H, and (d) blue class, feature z_S.

On the one hand, regarding the red class, studies have shown that the brick distribution in HS plane is mainly located in the lower hue values and does not fully overlap with that of traffic signs (see Fig. 3, extracted from [3]). Saturation values, in contrast, are non-discriminative. This was confirmed by tests conducted on our own set of images, and thereby a Gaussian function modeling the probability of a pixel to be a brick is added to the background class likelihood on the hue feature.

An analogous procedure is used to model the probability of a pixel to be part of the sky. Namely, from a set of images extracted from our sequence database, the features z_H and z_S are measured, and Gaussian distributions are adjusted to these data. In this case both hue and saturation turn out to be meaningful for separation between traffic signs and sky.

Once distributions for brick and sky are determined, the likelihood of the background is defined by a mixture model, both for $p(z_H|X_{BG})$ and $p(z_S|X_{BG})$, as follows:

$$p(z_H|X_{BG}) = \frac{1}{3}\left(\sum_{j\in\{H_{brick},H_{sky}\}} \frac{1}{\sigma_j\sqrt{2\pi}} e^{-\frac{1}{2}\left(\frac{z_H-\mu_j}{\sigma_j}\right)^2} + U(0,1)\right) \quad (4)$$

$$p(z_S|X_{BG}) = \frac{1}{2}\left(\frac{1}{\sigma_{S_{sky}}\sqrt{2\pi}} e^{-\frac{1}{2}\left(\frac{z_S-\mu_{S_{sky}}}{\sigma_{S_{sky}}}\right)^2} + U(0,1)\right) \quad (5)$$

where $U(0,1)$ represents a uniform distribution between 0 and 1 (which is the valid domain for both H and S components), and $(\mu_{H_{brick}}, \sigma_{H_{brick}})$, $(\mu_{H_{sky}}, \sigma_{H_{sky}})$ and $(\mu_{S_{sky}}, \sigma_{S_{sky}})$ are the parameters of the hue distribution for bricks, and of the hue and saturation distributions for the sky, respectively. The factors $1/3$ and $1/2$ ensure that the distributions integrate to one. The mixture model for the background likelihood is illustrated in Fig. 3: the hue profile comprises the uniform component and two Gaussian peaks modeling brick-like elements and sky, whereas the saturation is composed of a uniform term and a Gaussian function in the low z_S values corresponding to the sky.

An example of the result of the proposed color-based segmentation is shown in Fig. 5. Pixels classified as belonging to red and blue traffic signs are painted in white in Fig. 5 (d) and (e), respectively. The figure also illustrates the improvements of the proposed method compared to the use of a uniform background distribution (Fig. 5 (b) and (c)). As can be observed, the influence of disturbing background elements is considerably reduced, while the traffic signs remain clearly visible as elements of interest.

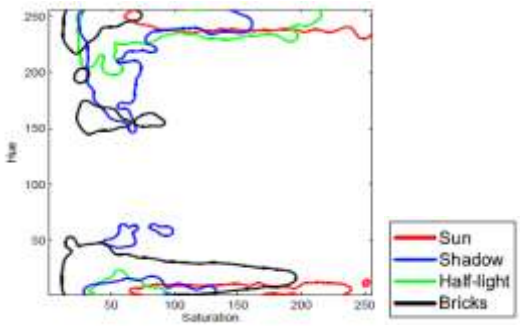

Fig. 3. HS distribution for red road signs (under different illumination conditions) and bricks.

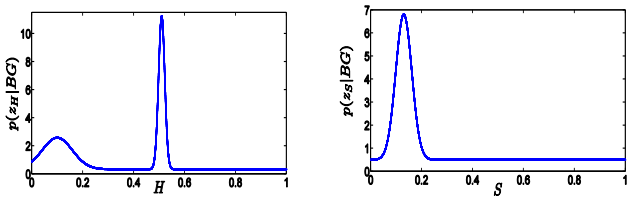

(a) (b)

Fig. 4. Likelihood distributions for background class: (a) for fetaure z_H, (b) for feature z_S.

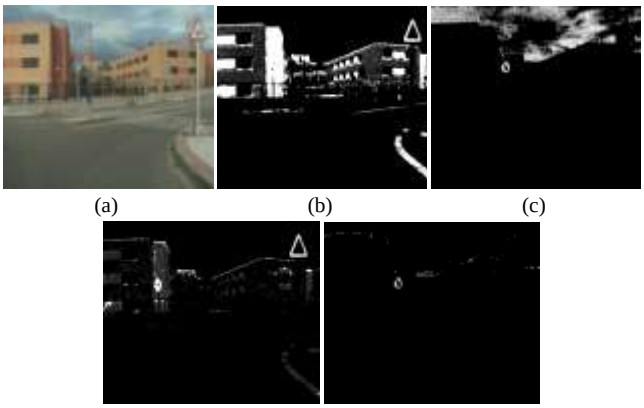

(a) (b) (c)

(d) (e)

Fig. 5. Result of color-based segmentation for the example image in (a). The result of using a uniform background distribution is shown in (b) and (c) for red and blue classes, respectively (the whiter the higher the probability of a pixel to be a TS). The corresponding result for the proposed framework is shown in (d) and (e). Observe that the amount of brick and sky pixels classified as TS is dramatically reduced, while the actual TS pixels are preserved.

IV. Region Analysis

After color analysis, the probability of the candidates to be TSs is further assessed through an additional region-level modeling. First, color-segmented images are binarized, and 8-connected components analysis is applied to them for candidate region labeling. TS characterization at region level involves modeling of the following parameters: TS area, pictogram area (both in pixels) and aspect ratio (width-to-height). We use a cascade of classifiers to significantly speed up the analysis. Each classifier deals with one of the abovementioned parameters and is designed to be simple and fast.

In the case of the TS area and the TS pictogram area, the range of valid values for both parameters is determined taking into account that: (i) a TS has to have a minimum size to be clearly visible in the image, and (ii) a valid TS cannot exceed a certain maximum size. These minimum and maximum size values have been experimentally determined considering a large set of images acquired with different camera settings whose fields of view are able to record signals appearing both at the left and right road sides. The profile inferred from experiments for these two parameters is similar to that shown in Fig. 6. For the TS area, $\mu_{Area} = 850$ and thresholds are set to $Th_j = 700$ and $Th_j^+ = Th_j + 30$, whereas for TS pictogram area, $\mu_{PicArea} = 500$, $Th_j = 450$ and $Th_j^+ = Th_j + 30$ as well.

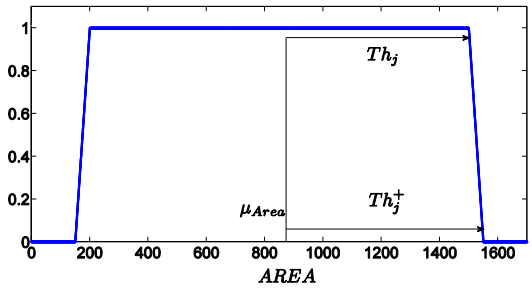

Fig. 6. Profile followed by the valid range of values for Area and Pictogram Area.

Concerning the TS aspect ratio, this parameter has been found to be very efficient to identify non-TS regions. Following the standard design of road signs, the theoretical value of the aspect ratio is the unity. However, perspective effects and rotations (especially in yaw angle for road signs, see Fig. 7 (a)) make this value significantly lower in most cases. Therefore, there is an interval of aspect ratio values, $[th_{ar}, 1]$ for which regions should be considered as potential TSs with the maximum probability. Beyond these thresholds the probability is linearly reduced until it reaches zero, meaning that the region is not accepted as a candidate TS. Different decreasing slopes are considered for the upper and lower end values as it is empirically verified that the uncertainty determining the lower threshold, th_{ar}, is higher than that for the upper one. Fig. 7 (b) shows the TS probability profile with respect to the aspect ratio with $th_{ar} = 0.65$.

V. TRACKING

In the previous stage, a set of candidate regions (hypotheses) have been generated which are likely to hold TSs. These ROIs are defined by their bounding boxes (BB). Monitoring their evolution along time can significantly enrich the accuracy of the detection results two-fold: (i) discarding those hypotheses which do not follow the expected TSs evolution patterns; (ii) updating the prior probabilities for the color analysis stage in the image areas where TSs are expected to be located.

Therefore, we introduce the regions resulting from the hypothesis generation stage –characterized by their bounding boxes– into a verification stage controlled by a Kalman filter associated to each candidate region in order to provide temporal coherence and improve the robustness of the decision making module. The designed filter is defined by the following parameters:

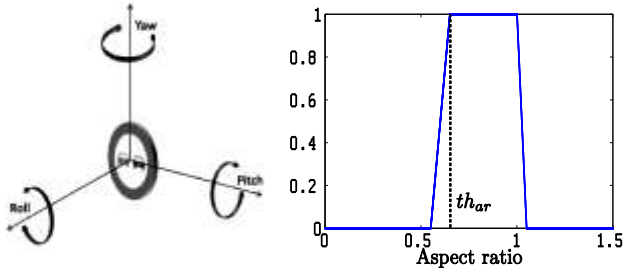

(a) (b)

Fig. 7. (a) The three TS possible rotation axes; (b) TS probability profile with respect to aspect ratio.

$$\boldsymbol{x}_k = (x, y, \dot{x}, \dot{y}, c, \dot{c}, ar)^{\mathrm{T}} \qquad \boldsymbol{z}_k = (x, y, c, ar)^{\mathrm{T}}$$

$$\mathrm{A} = \begin{pmatrix} 1 & 0 & 1 & 0 & 0 & 0 & 0 \\ 0 & 1 & 0 & 1 & 0 & 0 & 0 \\ 0 & 0 & 1 & 0 & 0 & 0 & 0 \\ 0 & 0 & 0 & 1 & 0 & 0 & 0 \\ 0 & 0 & 0 & 0 & 1 & 1 & 0 \\ 0 & 0 & 0 & 0 & 0 & 1 & 0 \\ 0 & 0 & 0 & 0 & 0 & 0 & 1 \end{pmatrix} \qquad \mathrm{H} = \begin{pmatrix} 1 & 0 & 0 & 0 & 0 & 0 & 0 \\ 0 & 1 & 0 & 0 & 0 & 0 & 0 \\ 0 & 0 & 0 & 0 & 1 & 0 & 0 \\ 0 & 0 & 0 & 0 & 0 & 0 & 1 \end{pmatrix}$$

where $\boldsymbol{x}_k$ represents the state vector, $\boldsymbol{z}_k$ the measurement vector, A is the state transition matrix and H is the matrix relating $\boldsymbol{x}_k$ and $\boldsymbol{z}_k$. In $\boldsymbol{x}_k$, x and y are the coordinates of the upper left corner of the region BB, c represents its width, $\dot{x}$, $\dot{y}$ and $\dot{c}$ their respective velocities, and ar its aspect ratio. These equations involve a first-order linear model for the TS position and width, and a zero-order linear model for its aspect ratio

In Fig. 8 we can see an example of the process which the filter aims to model. Several considerations shall be made as to the design of the filter. On the one hand, when the distance between the vehicle and the TS is high, parameters evolution can be assumed approximately linear, thus the Kalman filter is well adapted to the problem. In this case, the process noise is low (due to the linear behavior of the process) and lower than that of the measurements (measurements are not very reliable because of the high distance between the camera and the TS).

On the other hand, as the distance between the TS and the vehicle decreases, the evolution of the state parameters deviates from linearity. Therefore, process noise increases (reflecting the lack of linearity of the modeled process), and measurement noise decreases (measurements accuracy increases as TSs get closer to the vehicle).

We propose an innovative noise treatment that takes into account the abovementioned considerations: process and measurement noise covariance matrices, Q and R respectively, usually assumed to be constant [6], are modified to reflect the loss of linearity and the increase in measurement accuracy as candidate TSs get closer to the vehicle. They are modified based on the BB height increase rate between frames (time cannot be considered as TS evolution depends on the vehicle speed). This rate, denoted r_h, follows a quasi-linear pattern when the TS is far away located from the vehicle and diverges from it when it gets closer, as shown in Fig. 9 (a). Fig. 9 (b) shows how the process noise variance σ_q ($Q = \sigma_q \cdot I$) in red, and the measurement noise σ_r ($R = \sigma_r \cdot I$) in blue are modified in time according to r_h.

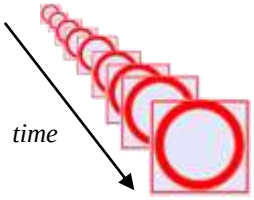

Fig. 8. Temporal evolution for an example TS.

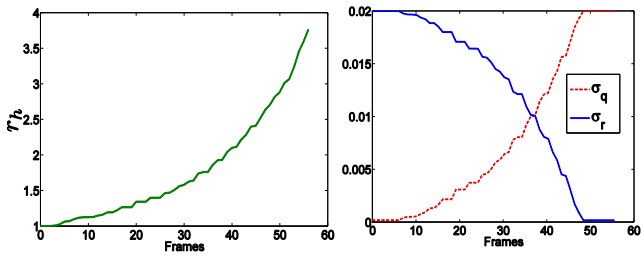

(a) (b)

Fig. 9. (a) Noise evolution, and (b) BB height evolution.

The aspect ratio parameter must be considered separately. As a matter of fact, it should be virtually constant in time unless the camera suffers abrupt rotation (if so its variation would still be small). Aspect ratio is therefore modeled to be constant for candidate BBs with a very small process noise (which is constant and smaller than the measurement noise regardless of time).

In order to decide whether the candidate is a road sign or not, we consider all the previously analyzed information (spatial and temporal). For each tracked region the decision module evaluates both the object area evolution and its trajectory. First, if a tracked object is a road sign, its area should not decrease with time (road sign is fixed in pavement and the vehicle approaches to it). On the other hand, the road sign position within the image should not change abruptly from one frame to the next. Thus, the trajectory described by a road sign is expected to be smooth. In conclusion, a region which is being tracked is considered to be a traffic sign if its area evolution is as explained and its trajectory is smooth enough.

Besides, as was mentioned previously, filtered results on I_k provide a prediction of where BBs are likely to be located in the next image, I_{k+1}. We propose using this information two-fold. First, we will utilize it to project the posterior probabilities ($P(X_i|\boldsymbol{z})$) of a pixel $\boldsymbol{z} = \{z_H, z_S\}$ to belong to the class $X_i \in \{R, B, BG\}$ at time k as prior probabilities at time $k+1$. This way, temporal coherence is exploited through a feedback loop within the Bayesian classification framework, thus improving traffic signs delineation. Second, predictions can be used whenever a TS is not found in the current image due to instantaneous occlusion, so that tracking of the TS is not interrupted.

VI. Results

Our experimental data consisted of more than one hour of video sequences, acquired from a video camera installed in a moving vehicle. The sequences contain 287 road signs in both highways and urban environments, involving variable illumination conditions and other effects such as rotation, occlusions, different vehicle velocities, etc. In TABLE I the detection rates achieved for highways and urban environments is presented. The only misdetections are due to extreme illumination conditions (such as very strong shadows or dazzling, see examples in Fig. 10) which render unpredictable color components, H and S, and which naturally cannot be addressed unless a prior pre-processing stage is introduced.

TABLE I
Summary of Results

Detection rate		
Highways	Urban environments	Total
92.3% (156/169)	98.3% (116/118)	94.8% (272/287)

Fig. 10. Example of misdetections due to shadows (left) and dazzling (right).

On the other hand, using the proposed approach no false positive has been observed throughout the sequence. These results prove the effectiveness of the algorithm, and reveals that through the combination of a set of simple features (color, area, and aspect ratio) the accuracy and robustness of the algorithm is significantly improved.

Results for the image in Fig. 5 (a) are shown in Fig. 11, where bounding boxes are drawn for the detected ROIs. As can be observed, regions that do not fit the size and aspect ratio constraints (e.g. building borders) are rejected. In particular, one important consequence of the designed region model is that, due to the constraint in aspect ratio, we are able to filter out TSs that are not oriented towards the vehicle (thus not affecting the driving) and which could mislead the driver, as it happens in Fig. 11 (a) for the red "no entry" TS.

In Fig. 12 (b) we can see the result of color and region analysis for another sample image (Fig. 12 (a)). As can be observed, the only detected ROI corresponds to the road sign. Again, we are able to filter out other regions that fit the color model thanks to the proposed model. Indeed, none of the other blue objects apart from the road sign have an inner pictogram and those situated lower in the image, in addition, do not fulfill the aspect ratio requirement.

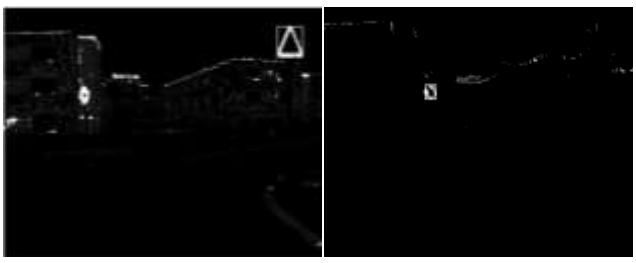

(a) (b)

Fig. 11. Results after color and region analysis for image in Fig. 5 for (a) red class, and (b) blue class.

(a) (b)

Fig. 12. Image in (b) shows the region detected for image in (a) after color and region analysis.

Fig. 13. Example of two TS tracking for a test sequence under good illumination.

Fig. 14. Example of TS tracking for a test sequence under bad illumination.

In Fig. 13 we can see the results of the complete traffic sign detection system for a test sequence, which contains several road signs (both red and blue) in different positions in a complex urban environment (comprising bricks and sky) under good illumination conditions. The road signs oriented towards the vehicle are perfectly detected and accurately located along the sequence.

Finally, we show an example (Fig. 14) of detection under poor illumination conditions (the road sign is located in a shadow region). Since these conditions have been considered during the design of the color analysis stage, the system is able to accurately handle it and detect the traffic sign.

VII. Conclusions

The proposed method has proven to provide excellent traffic sign detection and tracking results. Therefore, it can be used to enhance the performance of the posterior recognition stage, traditionally addressed through machine learning techniques. The main contribution of our approach is the use of a recursive Bayesian decision framework that allows to easily combine information of different nature, such as HS color at pixel level, and temporal and spatial coherence of image regions. Tests in both highways and urban environments yield an average detection rate above 94% for challenging situations, including illumination changes, clutter and rapid vehicle motion.

References

[1] A. de la Escalera, L. Moreno, M. Salichs and J. M. Armingol, "Road traffic sign detection and classification," *IEEE Transactions on Industrial Electronics*, vol. 44, pp. 848–859, Dec. 1997.

[2] A. Arlicot, B. Soheilian and N. Paparoditis, "Circular road sign extraction from street level images using colour, shape and texture database maps", CMRT09–IAPRS, vol. XXXVIII, Part 3/W4, pp. 205-211, Paris, France, Sept. 2009.

[3] J. P. Carrasco, A. de la Escalera and J. M. Armingol, "Driving supervision through traffic sign analysis," in *Proc. IEEE International Conference on Vehicular Electronics and Safety*, Columbus, OH, USA, Sept. 22–24, 2008, pp. 242–247.

[4] Y. Damavandi and K. Mohammadi, "Speed limit traffic sign detection and recognition", in *Proc. IEEE Conference on Cybernetics and Intelligent Systems*, Singapore, Dec. 1–3, 2004, pp. 797–802.

[5] C.-Y. Fang, S.-W. Chen and C.-S. Fuh, "Road-sign detection and tracking," *IEEE Transactions on Vehicular Technology*, vol. 52, pp. 1329–1341, Sept. 2003.

[6] A. A. Farag and A. E. Abdel-Hakim, "Detection, categorization and recognition of road signs for autonomous navigation," in *Proc. Advanced Concepts for Intelligent Vision Systems*, Brussels, Belgium, Aug. 31–Sep. 3, 2004, pp. 125–130.

[7] L. D. López and O. Fuentes, "Color-based road sign detection and Tracking," in *Proc. International Conference on Image Analysis and Recognition*, LNCS 4633, vol. 4633/2007, pp. 1138–1147, 2007.

[8] G. Loy and N. Barnes, "Fast shape-based road sign detection for a driver assistance system," in *Proc. IEEE/RSJ International Conference on Intelligent Robots and Systems*, Sendai, Japan, Sept. 28–Oct. 2, 2004, vol. 1, pp. 70–75.

[9] S. Maldonado-Bascon, S. Lafuente-Arroyo, P. Siegmann, H. Gomez-Moreno and F. Acevedo-Rodriguez, "Traffic sign recognition system for inventory purposes," in *Proc. IEEE Intelligent Vehicles Symposium*, Eindhoven, The Netherlands, June 4–6, 2008, pp. 590–595.

[10] R. Malik, J. Khurshid and S. Ahmad, "Road sign detection and recognition using colour segmentation, shape analysis and template matching," in *Proc. Int. Conference on Machine Learning and Cybernetics*, Hong Kong, 19–22 Aug., 2007, vol. 6, pp. 3556–3560.

[11] G. Piccioli, E. D. Micheli and M. Campani, "A robust method for road sign detection and recognition," in *Proc. European Conf. on Computer Vision*, Stockholm, Sweden, May 2-6, 1994, pp. 495–500.

[12] L. Yi-Sheng, D. Der-Jyh, C. Shu-Yuan, L. Ru-Sheng and H. Jun-Wei, "Scale and skew-invariant road sign recognition," *Int. Journal of Imaging Systems and Technology*, vol. 17, pp. 28–39, June 2007.